

## **A reduced dynamical model of convective flows in tall laterally heated cavities**

A. Liakopoulos, P. A. Blythe and H. Gunes

*Proc. R. Soc. Lond. A* 1997 **453**, 663-672

doi: 10.1098/rspa.1997.0037

---

### **Email alerting service**

Receive free email alerts when new articles cite this article - sign up in the box at the top right-hand corner of the article or click [here](#)

---

To subscribe to *Proc. R. Soc. Lond. A* go to: <http://rspa.royalsocietypublishing.org/subscriptions>

---

# A reduced dynamical model of convective flows in tall laterally heated cavities

BY A. LIAKOPOULOS, P. A. BLYTHE AND H. GUNES

*Department of Mechanical Engineering and Mechanics, Lehigh University,  
Bethlehem, PA 18015-3085, USA*

Proper orthogonal decomposition (the Karhunen–Loève expansion) is applied to convective flows in a tall differentially heated cavity. Empirical spatial eigenfunctions are computed from a multicellular solution at supercritical conditions beyond the first Hopf bifurcation. No assumption of periodicity is made, and the computed velocity and temperature eigenfunctions are found to be centro-symmetric. A low-dimensional model for the dynamical behaviour is then constructed using Galerkin projection. The reduced model successfully predicts the first Hopf bifurcation of the multicellular flow. Results determined from the low-order model are found to be in qualitative agreement with known properties of the full system even at conditions far from criticality.

---

## 1. Introduction

Construction of low-dimensional models of transitional and turbulent flows by reduction of the governing partial differential equations to minimal systems of ordinary differential equations has attracted significant attention in recent years (Berkooz *et al.* 1993). Low-dimensional models offer a compact description of the system dynamics, and they are potentially useful in designing, simulating, and testing flow control systems. In general, the transformation of partial differential equations into systems of ordinary differential equations can be accomplished by well-established procedures. The method of weighted residuals, for example, has been successfully used in conjunction with a variety of basis functions, such as splines (Liakopoulos & Hsu 1984) or, more frequently, trigonometric functions and orthogonal polynomials (Gottlieb & Orszag 1977). In practice, the infinite-dimensional representation is truncated to a finite  $n$ -dimensional system. To ensure that the dynamical behaviour described by the resulting finite-dimensional system corresponds to that of the full problem, the required dimension  $n$  is typically high; a large reduction in  $n$  is required for the development of useful low-order models. This can be accomplished by expanding the unknown functions in terms of basis functions that are constructed specifically for each flow system and that reflect the behaviour of the flow in the vicinity of specified values of the controlling parameters. A systematic procedure for obtaining a set of optimal basis functions (Berkooz *et al.* 1993) is proper orthogonal decomposition (POD), first proposed in fluid mechanics by Lumley (1967) as a tool for the identification of coherent structures in turbulent flows. An efficient and cost-effective method of applying proper orthogonal decomposition to large data sets was developed by Sirovich (1987) who devised what has become known as the snapshot

method. POD identifies the most energetic eigenmodes, thus enabling the compression of numerical or experimental data by retaining the small number of modes that capture most of the fluctuation ‘energy’. The most energetic eigenmodes should contain enough information for a satisfactory description of the flow dynamics. This methodology has been applied to a variety of problems including: the dynamics of coherent structures in the turbulent wall layer (Aubry *et al.* 1988), and the evolution of three-dimensional coherent structures in a flat-plate boundary layer (Rempfer & Fasel 1994). Deane *et al.* (1991) reported a low-dimensional model of two-dimensional flow in a grooved channel, while Gunes *et al.* (1997) discussed low-dimensional representations of transitional, buoyancy-driven flows in vertical channels. For a detailed discussion of POD and its applications, see Berkooz *et al.* (1993).

In most applications, proper orthogonal decomposition has been carried out for flows that are periodic in at least one spatial direction, and low-dimensional models have been developed for some of these cases. Sirovich & Park’s work on Rayleigh-Benard convection in a finite domain (Sirovich & Park 1990) is a notable exception. These authors discuss proper orthogonal decomposition for convection in a low-aspect-ratio domain with stressless (slippery) boundary conditions at fixed values of the controlling parameters. The present paper explores the possibility of developing POD-based low-order models of thermal convection in extended systems, where the interplay between temporal and spatial instabilities is far more complex and interesting. Specifically thermal convection in a tall laterally heated cavity is examined using the exact (no-slip) flow boundary conditions along the enclosure walls. Furthermore, an effort is made to explore the properties of the resulting low-dimensional model at various forcing conditions. The combination of realistic flow and thermal boundary conditions, with a large aspect-ratio geometry, is relevant to a variety of materials processing and cooling applications.

For a Newtonian fluid, subject to the Boussinesq approximation, thermal convection in a rectangular cavity when the vertical boundaries are maintained at fixed but distinct temperatures, and the upper and lower horizontal surfaces are adiabatic, is governed by three dimensionless parameters: the aspect ratio  $A$  (height/width), the Prandtl number  $Pr$ , and the Grashof number  $Gr$  (Batchelor 1954). At moderate  $Gr$ , the base flow corresponds to a single unicellular state. Depending on the aspect ratio and Prandtl number, both time-dependent and stationary bifurcations can occur as  $Gr$  increases. For air-filled cavities of small aspect ratio, the primary instability leads to oscillatory time-dependent flow (Paolucci & Chenoweth 1989). Calculations by Lee and Korpela (1983) suggest that at values of  $A \geq 12.5$  a stationary instability will certainly precede the onset of oscillatory convection, and give rise to a steady (time-independent) multicellular flow. Further increase in  $Gr$  leads to oscillatory flow or a reduction in the number of cells. Detailed calculations of the supercritical cell structure have been given by Chait & Korpela (1989) and by Liakopoulos *et al.* (1990).

In this paper POD is applied to thermal convection in a tall differentially heated cavity, and the possibility of developing low-dimensional models to describe the dynamics of multicellular flows is investigated. Results are presented for transitional flow in an air filled cavity of aspect ratio  $A = 40$ . The spatial eigenmodes are determined by the method of snapshots at  $Gr_o = 25000$  and  $Pr_o = 0.71$ . A Galerkin procedure is then employed to obtain suitable low-order dynamical models. Assuming that the spatial eigenfunctions are weak functions of  $Gr$ , the properties of the derived low-dimensional model are explored for values of  $Gr \neq Gr_o$ . This study is carried out at  $Pr = 0.71$ .

## 2. Full model

Two-dimensional thermal convection is examined in a cavity of aspect ratio  $A = 40$ . The side walls are maintained at uniform but distinct temperatures, while the upper and lower horizontal walls are thermally insulated. Suitable dimensionless variables are

$$(x, y) = \frac{(x^*, y^*)}{l}, \quad t = \frac{u_c}{l} t^*, \quad \mathbf{V} = \frac{\mathbf{V}^*}{u_c}, \quad P = \frac{p^*}{\rho u_c^2}, \quad \Theta = \frac{T - T_1}{T_2 - T_1}, \quad (2.1)$$

where  $u_c = \sqrt{\beta g l (T_2 - T_1)}$ ,  $l$  is the cavity width,  $\rho$  is the fluid density,  $T_1$  and  $T_2$  are the cold and hot wall temperatures,  $\beta$  is the thermal expansion coefficient, and  $g$  is the acceleration due to gravity. Note that since the analysis is concerned with modelling the transitional flow regime ( $Gr > Gr^*$  where  $Gr^*$  denotes the Grashof number at the onset of self-sustained oscillations), the characteristic velocity  $u_c$  is determined by balancing the inertial and buoyancy forces in the momentum equation and the pressure is scaled by the dynamic pressure measure  $\rho u_c^2$ . It is hoped that this scaling will represent the flow behaviour over a reasonable range of Grashof numbers.

In terms of the variables listed in (2.1) and, using the Boussinesq approximation, the dimensionless governing partial differential equations take the form

$$\nabla \cdot \mathbf{V} = 0, \quad (2.2)$$

$$\frac{\partial \mathbf{V}}{\partial t} + (\mathbf{V} \cdot \nabla) \mathbf{V} + \nabla P = \theta \mathbf{j} + \frac{1}{\sqrt{Gr}} \nabla^2 \mathbf{V}, \quad (2.3)$$

$$\frac{\partial \Theta}{\partial t} + \mathbf{V} \cdot \nabla \Theta = \frac{1}{Pr \sqrt{Gr}} \nabla^2 \Theta, \quad (2.4)$$

where  $Pr = \nu/\alpha$  is the Prandtl number,  $Gr = \beta g (T_2 - T_1) l^3 / \nu^2$  is the Grashof number,  $\nu$  is the kinematic viscosity,  $\alpha$  is the thermal diffusivity, and  $\mathbf{j}$  is the unit vector in the vertical  $y$ -direction. For a rectangular coordinate system with the origin at the midpoint of the left vertical wall, the associated boundary conditions are  $\mathbf{V} = \mathbf{0}$  along all cavity walls,  $\Theta = 1$  at  $x = 0$ ,  $\Theta = 0$  at  $x = 1$ , and  $\partial \Theta / \partial y = 0$  at  $y = \pm \frac{1}{2} A$ .

## 3. Derivation of the low-order model

At some values  $(Pr_o, Gr_o)$  for which the flow and temperature fields are spontaneously oscillatory,  $M$  snapshots of each field are computed from the full model described in the previous section. The values  $(Pr_o, Gr_o)$  are referred to as ‘design’ parameters or ‘design’ conditions. The time-dependent velocity and temperature data are decomposed into time-averaged  $(\bar{u}, \bar{v}, \bar{\Theta})$  and time-varying  $(u', v', \Theta')$  parts, where  $(u, v)$  are the components of  $\mathbf{V}$  along the rectangular coordinate axes  $x$  and  $y$  respectively.

Stationary empirical eigenfunctions  $(\phi_k, \psi_k)$ , are constructed from linear combinations of the time varying parts of the field variables (Sirovich 1987), i.e.

$$\phi_{\mathbf{k}}(x, y) = \sum_{i=1}^M \alpha_{ki} \mathbf{V}'_i, \quad (3.1)$$

$$\psi_k(x, y) = \sum_{i=1}^M \alpha_{ki} \Theta'_i, \quad (3.2)$$

where the subscript  $i$  refers to the fluctuation fields obtained at  $t = t_i$ . In (3.1) and (3.2),  $\alpha_k$  denotes the  $k$ th eigenvector of the matrix eigenvalue problem

$$\mathbf{C}\boldsymbol{\alpha} = \lambda\boldsymbol{\alpha}, \quad (3.3)$$

where  $\mathbf{C}$  is a  $M \times M$  matrix given by

$$C_{ij} = \frac{1}{M} \iint \mathbf{V}'_i \cdot \mathbf{V}'_j \, d\Omega \quad (3.4)$$

for the velocity field, and

$$C_{ij} = \frac{1}{M} \iint \Theta'_i \Theta'_j \, d\Omega \quad (3.5)$$

for the temperature field. Integration is over the spatial flow domain  $\Omega$ .

Note that the matrix  $\mathbf{C}$  is symmetric and positive semi-definite. Consequently, all eigenvalues are real and non-negative and can be ordered such that

$$\lambda_1 \geq \lambda_2 \geq \lambda_3 \geq \dots \geq \lambda_M.$$

Each velocity eigenvalue represents the contribution of the corresponding eigenmode to the mean of the total fluctuation energy

$$E = \iint (u'^2 + v'^2) \, d\Omega,$$

while each temperature eigenvalue represents the contribution of the corresponding temperature mode to the mean of the total temperature fluctuation ‘energy’

$$E_\Theta = \iint \Theta'^2 \, d\Omega.$$

Proper orthogonal decomposition offers an objective method for the identification of the most energetic eigenfunctions,  $(\phi_i, \psi_i)$ ,  $i = 1, 2, \dots, M_c$ , where  $M_c$  is problem dependent. The eigenfunctions are mutually orthogonal and, when properly normalized,  $(\phi_i \rightarrow \phi_i/\sqrt{\lambda_i}, \psi_i \rightarrow \psi_i/\sqrt{\lambda_i})$ , they form an orthonormal basis.

The time-varying parts of the velocity and the temperature fields are expanded in terms of the normalized eigenfunctions,

$$\mathbf{V}' = \sum_{k=1}^{M_1} a_k(t) \phi_k(x, y), \quad (3.6)$$

$$\Theta' = \sum_{k=1}^{M_2} b_k(t) \psi_k(x, y), \quad (3.7)$$

where by taking into account the orthonormality conditions satisfied by the eigenfunctions, the temporal expansion coefficients  $a_k(t)$  and  $b_k(t)$  can be calculated from

$$a_k(t) = \iint \mathbf{V}' \cdot \phi_k \, d\Omega, \quad k = 1, 2, \dots, M_1 \quad (3.8)$$

and

$$b_k(t) = \iint \Theta' \psi_k \, d\Omega, \quad k = 1, 2, \dots, M_2. \quad (3.9)$$

Expressions (3.6)–(3.9) are referred to as the reconstruction formulae.

Substituting (3.6)–(3.7) into the momentum and energy equations, (2.3) and (2.4),

applying Galerkin's method, and making use of the orthonormality property of the empirical eigenfunctions, leads to a system of  $(M_1 + M_2)$  nonlinear ODEs for the temporal expansion coefficients:

$$\frac{da_k}{dt} = A_k + \frac{1}{\sqrt{Gr}}B_k + C_{ki}a_i + \frac{1}{\sqrt{Gr}}D_{ki}a_i + E_{kij}a_i a_j + R_{ki}b_i, \quad (3.10)$$

$$k = 1, 2, \dots, M_1,$$

$$\frac{db_k}{dt} = F_k + \frac{1}{Pr\sqrt{Gr}}G_k + H_{ki}a_i + \frac{1}{Pr\sqrt{Gr}}I_{ki}b_i + J_{kij}a_i b_j + K_{ki}b_i, \quad (3.11)$$

$$k = 1, 2, \dots, M_2.$$

The coefficients in the above equations are related to various inner products among the eigenfunctions and to certain properties of the mean flow. Specific results for these coefficients can be obtained from the authors. Note that the velocity eigenfunctions are, by construction, divergence-free and that the continuity equation is automatically satisfied.

Equations (3.10) and (3.11) are of the form  $\dot{x} = c + Lx + N(x)$ , where  $x$  denotes the  $n$ -vector of the modal amplitudes,  $c$  is a constant  $n$ -vector, and  $L$  is an  $n$  by  $n$  matrix that has contributions from the Laplacians in the full model equations and from the interactions of the mean fields with the fluctuations. The nonlinear operator  $N$  is quadratic in  $x$ , a typical outcome when the Galerkin method is applied to the Boussinesq equations. Initial conditions for the design state are obtained by applying (3.8) and (3.9) at  $t = 0$ .

#### 4. Decomposition

The partial differential equations (2.2)–(2.4), together with no-slip boundary conditions at all walls, isothermal conditions along the vertical walls, and adiabatic conditions along the horizontal walls, are solved by a spectral element method. Implementation of the method is based on Nekton, a program developed by Patera and his co-workers for the simulation of steady and unsteady incompressible flow, including heat and mass transfer. In the present simulations 170 spectral elements are used and solutions are obtained for order of interpolants  $N_1 = 4, 6, 8, 10$ . Increasing  $N_1$  from 8 to 10 does not result in any significant change for  $Gr \leq 2.5 \times 10^4$ . Values of the field variables at representative fixed locations and integrals of the field variables over the entire domain change by less than 0.9% at  $Gr = 2.5 \times 10^4$ . The results reported in this article were obtained for  $N_1 = 10$ .

Proper orthogonal decomposition is carried out on 20 snapshots ( $M = 20$ ) of the oscillatory solution obtained for  $A = 40$ , at design conditions  $Pr = Pr_o = 0.71$  and  $Gr = Gr_o = 2.5 \times 10^4$ . The snapshots are equally spaced over the oscillation period. Representative instantaneous streamline and isotherm patterns are shown in figure 1*a*. Table 1 lists the six largest eigenvalues for the velocity and temperature fields. All eigenvalues are normalized so that  $\sum \lambda_i = 1$ . The cumulative contribution of the six most energetic eigenmodes to the total flow and temperature fluctuation energy are listed in the third and fifth columns of table 1. As can be seen from the table, the dominant velocity mode contributes 61.1% to the fluctuation energy, while the dominant temperature mode contributes 72.5% to the fluctuation 'energy' of the temperature field. Note that the four most energetic modes capture 99.98% of the total fluctuation energy for both the velocity and the temperature fields.

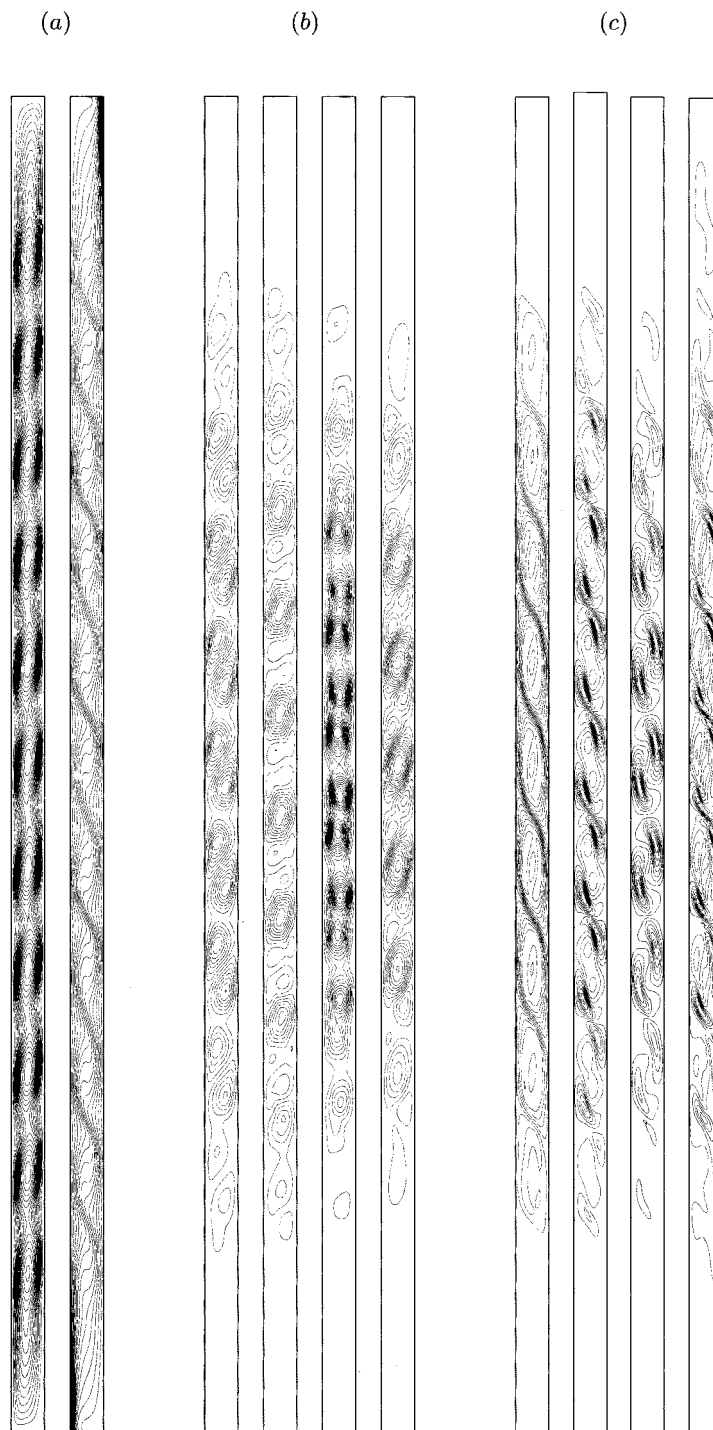


Figure 1. (a) Representative instantaneous streamlines and isotherms, (b) velocity eigenfunctions (streamlines), (c) temperature eigenfunctions (isotherms).

Table 1. *Eigenvalues of the six most energetic modes and their respective contribution to the total flow and temperature fluctuation ‘energy’*

mode	velocity eigenvalues		temperature eigenvalues	
	eigenvalue	cumul. energy	eigenvalue	cumul. energy
1	0.61103	61.103	0.72516	72.516
2	0.35078	96.181	0.26079	98.595
3	0.02426	98.607	0.01140	99.735
4	0.01371	99.978	0.00245	99.980
5	$0.136 \times 10^{-3}$	99.992	$0.111 \times 10^{-3}$	99.991
6	$0.068 \times 10^{-3}$	99.998	$0.655 \times 10^{-4}$	99.998

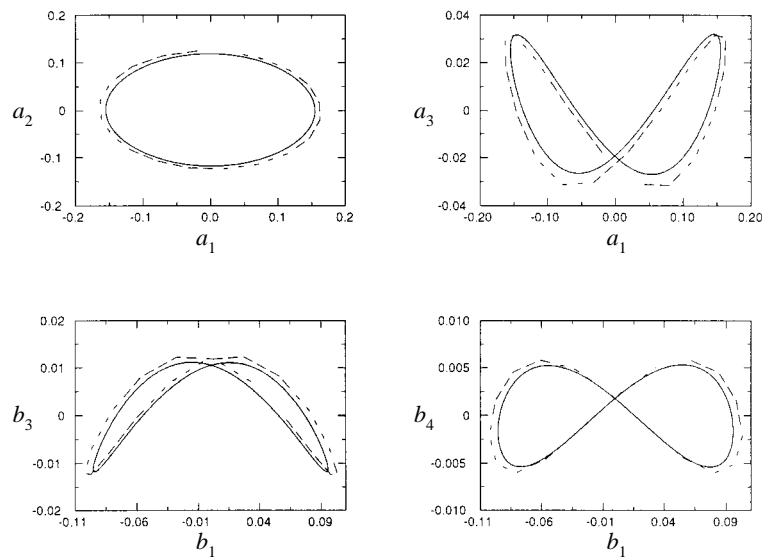


Figure 2. Phase space trajectories at design conditions. Solid line: low-dimensional model; dashed line: direct projection of snapshots on the computed eigenfunctions.

Streamlines and isotherms for the four most energetic eigenmodes are depicted in figures 1*b, c*. Organized spatial patterns in the most energetic eigenfunctions occur in the middle part of the cavity where the fluctuations are most vigorous. In addition, the eigenfunctions are centro-symmetric. Some minor violations of these conditions are evident, especially in the higher modes where computational noise masks the spatial symmetry relations. Steady solutions of (2.2)–(2.4) for the boundary conditions considered in this study are also centro-symmetric (Gill 1966).

### 5. Low-order model

The eight-equation model ((3.10)–(3.11),  $M_1 = M_2 = 4$ ) has been studied in detail. At design conditions, the initial-boundary value problem is solved by a fourth order Runge–Kutta method. For these conditions, a limit cycle is reached after all

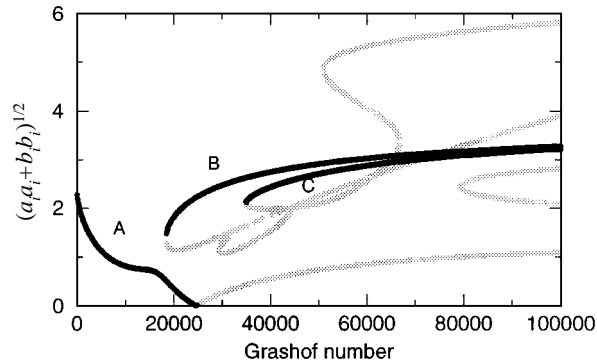


Figure 3. Fixed points of the low-dimensional model. Norm for  $M_1 = M_2 = 4$ . Black lines, stable fixed points; grey lines, unstable fixed points.

initial transients die out. Oscillation frequencies predicted by the low-order model are in excellent agreement with those obtained from the reconstruction formulae (3.8) and (3.9). Figure 2 depicts trajectories of the modal amplitudes in projections of the phase space. Clearly the temporal expansion coefficients predicted by the low-order model exhibit oscillations of slightly different amplitude than those calculated by direct projection of the input data onto the computed eigenfunctions. The equilibrium points (critical points, steady solutions) of the low-order model are found by setting the right-hand side of (3.10)–(3.11) to zero. Using a Newton–Raphson method, with random initial guesses for the solution components, several steady solution branches are found in the interval  $1 \leq Gr \leq 10^5$ . The stability of a steady solution is then determined by calculating the eigenvalues of the associated real non-symmetric Jacobian matrix evaluated at the critical point. Equilibrium points with norm smaller than 6 in the interval  $1 \leq Gr \leq 10^5$  are presented in figure 3. Black lines represent stable fixed points while gray lines correspond to unstable fixed points. For  $Gr < 1.85 \times 10^4$  a unique branch of stable fixed points is found. This is the primary solution branch and is denoted by A in figure 3, where the norm  $(a_i a_i + b_i b_i)^{1/2}$  is plotted against  $Gr$ . For  $Gr \geq 1.85 \times 10^4$  multiple solutions are found. Two stable steady solutions exist for  $1.85 \times 10^4 \leq Gr \leq 2.48 \times 10^4$ . At  $Gr = Gr_c = 2.48 \times 10^4$  the fixed point on the primary branch undergoes a Hopf bifurcation which marks the onset of periodic oscillations in time. For  $2.48 \times 10^4 \leq Gr \leq 3.49 \times 10^4$  one stable steady solution (branch B) is found, while for  $Gr \geq 3.49 \times 10^4$  two stable steady solutions exist (branches B and C). Note that the upper limit of  $Gr$  in figure 3 corresponds to  $(Gr - Gr_c)/Gr_c \approx 4$ , where  $Gr_c$  denotes the value of  $Gr$  at the onset of oscillations.

A systematic quantitative comparison between the full model and the low-dimensional model (LDM) predictions at off-design conditions is beyond the scope of this paper. Direct numerical simulation of the early transition process in the extended system under study is prohibitively expensive. Hysteresis effects make the determination of all states very complex. However, even far from design conditions, the LDM exhibits properties that are qualitatively in agreement with the full model results, for example, it predicts a unique stable steady solution for small values of  $Gr$ . In addition, it indicates the existence of a second stable steady solution before the first Hopf bifurcation point, in agreement with the fact that for  $A = 40$  and  $Pr = 0.71$  the first instability is a stationary instability. Further, for high values of  $Gr$  the LDM predicts multiple steady stable solutions, in agreement with the existence of multiple

stationary multicellular solutions, characterized by distinct numbers of cells, that are found in the flow system. At very high values of  $Gr$  the LDM exhibits chaotic behaviour. No claim of quantitative agreement far from the design conditions is made here but the qualitative comparison is encouraging. Obviously, the present approach requires that the empirical eigenfunctions be only weakly dependent on the normalized Grashof number  $(Gr - Gr_c)/Gr_c$ . This point is of considerable interest, and further analysis is certainly required. Extensions of the LDM to include a dependence on the normalized Grashof number is possible but, because of the extensive numerical work needed, it is deferred for future study. The present paper is intended as a preliminary investigation of the properties of the LDM near design conditions.

## 6. Conclusions

A POD-based low-dimensional model of thermal convection in a laterally heated rectangular enclosure has been presented. Appropriate nondimensional variables are defined by balancing inertial and buoyancy effects. The POD eigenfunctions, computed at slightly supercritical conditions, are centro-symmetric and provide a basis for the approximation of the velocity and temperature fluctuations required in the Galerkin projection. Frequency and amplitude predictions based on the developed low-dimensional model are in good agreement with the full model solutions at design conditions. Far from design conditions, the model exhibits properties that are qualitatively in agreement with the solutions of the partial differential equations. Obviously, the low-dimensional model is not expected to reproduce all properties of the full model solutions, and its ability to reproduce specific flow aspects is restricted to some range of the controlling parameters. Determination of this range is beyond the scope of this work, but the initial results already obtained are encouraging.

This work was partly supported by NASA/LeRC under contract NAG3-1632.

## References

- Aubry, N., Holmes, P., Lumley, J. L. & Stone, E. 1988 The dynamics of coherent structures in the wall region of a turbulent boundary layer. *J. Fluid Mech.* **192**, 115–173.
- Batchelor, G. K. 1954 Heat transfer by free convection across a closed cavity between vertical boundaries at different temperatures. *Q. Appl. Math.* **12**, 209–233.
- Berkooz, G., Holmes, P. & Lumley, J. L. 1993 The proper orthogonal decomposition in the analysis of turbulent flow. *A. Rev. Fluid. Mech.* **25**, 539–575.
- Chait, A. & Korpela, S. A. 1989 The secondary flow and its stability for natural convection in a tall vertical enclosure. *J. Fluid Mech.* **200**, 189–216.
- Deane, A. E., Kevrekidis, I. G., Karniadakis, G. E. & Orszag, S. A. 1991 Low dimensional models for complex geometry flows: application to grooved channels and circular cylinders. *Phys. Fluids A* **3**, 2337–2354.
- Gill, A. E. 1966 The boundary layer regime for convection in a rectangular cavity. *J. Fluid Mech.* **26**, 515–536.
- Gottlieb, D. & Orszag, S. A. 1977 *Numerical analysis of spectral methods*. Philadelphia, PA: Society for Industrial and Applied Mathematics.
- Gunes, H., Liakopoulos, A. & Sahan, R. A. 1997 Low-dimensional description of oscillatory thermal convection: the small Prandtl number limit. *Theor. Computat. Fluid Dynamics* **9**. (In the press.)
- Lee, Y. & Korpela, S. A. 1983 Multicellular natural convection in a vertical slot. *J. Fluid Mech.* **126**, 91–121.

- Liakopoulos, A., Blythe, P. A. & Simpkins, P. G. 1990 Convective flows in tall cavities. *Simulation and numerical methods in heat transfer* (ed. A. F. Emery), pp. 81–87. ASME-HTD, vol. 157.
- Liakopoulos, A. & Hsu, C. C. 1984 On a class of compressible laminar boundary-layer flows and the solution behaviour near separation. *J. Fluid Mech.* **149**, 339–353.
- Lumley, J. L. 1967 The structure of inhomogeneous turbulent flows. In *Atmospheric turbulence and radio wave propagation* (ed. A. M. Yaglom & V. I. Tatarski), pp. 166–178. Moscow: Nauka.
- Paolucci, S. & Chenoweth, D. R. 1989 Transition to chaos in a differentially heated vertical cavity. *J. Fluid Mech.* **201**, 379–410.
- Rempfer, D. & Fasel, H. F. 1994 Evolution of three-dimensional coherent structures in a flat-plate boundary layer. *J. Fluid Mech.* **260**, 351–375.
- Sirovich, L. 1987 Turbulence and the dynamics of coherent structures. I–III. *Q. Appl. Math.* **45**, 561–590.
- Sirovich, L. & Park, H. 1990 Turbulent thermal convection in a finite domain. I. Theory. *Phys. Fluids A* **2**, 1649–1658.

*Received 5 November 1996; revised 20 December 1996; accepted 17 January 1997*